1   # Supplemental Materials

Section 1: Refractive Broadening

This section of the supplement describes the background and methodology of extracting the dipolar-broadened linewidth of a resonance at high concentrations, where the measured lineshapes are affected by refractive broadening. This accounts for the same effect known as "propagation effect," which the authors found treated similarly in literature following submission.[1] Refractive broadening emerges in samples where the high concentration, large polarization and narrow linewidth cooperate to cause an extremely large change in sample susceptibility on resonance. This dramatic change in susceptibility alters the dielectric properties of the sample appreciably. When this occurs, the reflections from the sample are no longer simply proportional to the field-dependent susceptibility response as is the case at lower concentrations. As the 240 GHz EPR spectrometer measures the reflection from the sample (backed by a mirror), this means that when this occurs our measured signal is no longer identical to the field-dependent susceptibility response that we wish to measure. Therefore, we examine a method of determining the susceptibility response by explicitly calculating the reflection with the Fresnel equations. This allows us to approximate the shape of the susceptibility response that generated the measured reflection and use that to estimate the true dipolar-broadened linewidth.
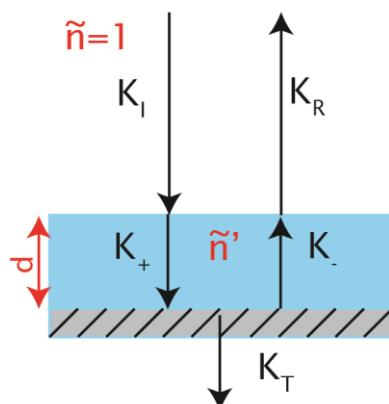

Figure S1: Sample Geometry. Shows the simplified geometry used for the calculation for a sample of thickness d. This three media setup shows wavevectors K_I and K_R of the incident and reflected fields in the waveguide (with index $\tilde{n}=1$). K_+ and K_- are the wavevectors of forward and backward moving waves within the sample, which has a complex, frequency (/field) dependent index of refraction ($\tilde{n}'$). Finally, K_T is the transmitted wave, which is assumed have zero amplitude as the sample is backed with a metallic mirror. Note the interfaces of the sample holder are ignored.

38

39   **1A) Calculation of Reflection from a Paramagnetic Sample**
40   We begin by examining the physical arrangement of our sample as shown in Fig. S1. We
41   approximate a flat sample of thickness d on top of a mirror. This ignores the sample holder,
42   which is made from Teflon, and thus should not have any response to the modulated field. This
43   also ignores any asymmetry in sample geometry or meniscus formed in the sample. We expect
44   that, while both effects may be present, this is still a sufficient approximation to develop an
45   understanding of our spectra.

1   The problem is then reduced to a two interface problem where we must satisfy two
2 boundary conditions. The first interface is between air and the sample for the incident and
3 reflected waves (given by wavevectors K_I and K_R) and the two waves propagating within the
4 sample (wavevectors K_+ and K_-). Additionally, the interface between the sample and mirror
5 requires the transmitted wave (with wave vector K_T) be zero. It is then a straightforward
6 calculation to express the reflection from this sample setup as a function of the sample's
7 permeability and permittivity.
8
9   .

$$R = \frac{E_R}{E_I} = X + \iota Y = \left[\frac{e^{2\iota\phi}\left(\sqrt{\epsilon_R\mu_{Air}} + \sqrt{\epsilon_{Air}\mu_R}\right) + \left(\sqrt{\epsilon_R\mu_{Air}} - \sqrt{\epsilon_{Air}\mu_R}\right)}{e^{2\iota\phi}\left(\sqrt{\epsilon_R\mu_{Air}} - \sqrt{\epsilon_{Air}\mu_R}\right) + \left(\sqrt{\epsilon_R\mu_{Air}} + \sqrt{\epsilon_{Air}\mu_R}\right)}\right]$$

$$\approx \left[\frac{e^{2\iota\phi}\left(\sqrt{\epsilon_R} + \sqrt{\mu_R}\right) + \left(\sqrt{\epsilon_R} - \sqrt{\mu_R}\right)}{e^{2\iota\phi}\left(\sqrt{\epsilon_R} - \sqrt{\mu_R}\right) + \left(\sqrt{\epsilon_R} + \sqrt{\mu_R}\right)}\right] \qquad (S1)$$

10
11 is the reflected signal calculated from the Fresnel Equations[2] and is a complex number
12 containing the in- and out-of-phase response of the spins as X and Y respectively. E_R and E_I are
13 the electric field strengths of the reflected and incident radiation respectively, ϕ is the phase
14 acquired by millimeter-wave radiation when passing through the sample, ϵ_{Air} and ϵ_R are the
15 permittivity of and air and the sample respectively, and μ_{Air} and μ_R are the permeability of air
16 and the sample respectively. We can express the phase acquired in terms of the known
17 parameters by $\phi = \frac{\omega d}{c}\sqrt{\epsilon_R\mu_R}$, where d is the sample thickness, and c is the speed of light. We
18 make the (accurate) approximation that $\mu_{Air} \approx \epsilon_{Air} \approx 1$. To determine the reflections we write
19 $\mu_{rel} = 1 + \chi$ where $\chi = \chi' + \iota\chi''$ is the complex susceptibility, and we take $\epsilon_{rel} \approx 3.2$ from the
20 permittivity of frozen ice[3]. We approximate the susceptibility response as a simple Lorentzian for
21 simplicity and so can write[4]

22
$$\chi' = \frac{\chi_0\,\omega_L}{2}\frac{\omega_L - \omega}{(\omega - \omega_L)^2 + \left(\frac{1}{T_2}\right)^2}$$

23
$$\chi'' = \frac{\chi_0\,\omega_L}{2T_2^*}\frac{1}{(\omega - \omega_L)^2 + \left(\frac{1}{T_2}\right)^2} \qquad (S2)$$

24   where χ_0 is the DC susceptibility of the spins, ω_L is the electron Larmor frequency, ω is
25 the irradiation frequency, and T_2 is the width of the resonance. We emphasize here that T_2 is only
26 a manner of characterizing the resonance width of the susceptibility in our approximation of a
27 homogeneous, Lorentzian lineshape and does not reflect the phase memory time in our samples.
28 By calculating the expected susceptibility response as a function of ω_L (which is given by the
29 swept magnetic field) this yields ϕ_R and μ_{Rel} (also as a function of ω_L). Then the expected signal
30 (real and imaginary parts) can be calculated as a function of ω_L through Eq. S1, giving us a
31 calculated spectrum to compare to those measured in experiment.
32   Our input parameters for these calculations are $\omega_L, \omega, T_2, \chi_0$ and d. It is clear that ω is
33 fixed by our irradiation frequency ($2\pi\cdot240$ GHz) and ω_L is fixed by the external magnetic field,
34 which is swept around 8.6 T. χ_0 is fixed by the spin species (S=7/2 for Gd^{3+}), concentration,
35 temperature and magnetic field as follows[4]

1 $$\chi_0 = \frac{N}{V}\mu_0\beta\left(g_J\mu_B J\right)^2\left(\frac{1}{4\,J^2}csch^2\left(\frac{1}{2}\beta g_J\mu_B B\right)\right.$$

2

3 $$\left.-\frac{(2J+1)^2}{4J^2}csch^2\left(\frac{2J+1}{2}\beta g_J\mu_B B\right),\right.$$ (S3)

4

5 where N/V is the spin concentration, J is the spin quantum number, g_j is the effective g-value of

6 the spins (g_j=1.992 for Gd^{3+}), μ_B is the Bohr Magneton, μ_0 is the vacuum permeability, $\beta = \frac{1}{kT}$

7 is the Boltzmann factor, and B is the external magnetic field.

8

9

10 **1B) Evaluating Calculated Spectra for $\bar{r}$=1.78 nm Samples**

11 Estimation of parameters based on calculations are only carried out for the $\bar{r}$=1.8 nm (50

12 mM) samples, as mentioned in the manuscript. Although we find sample geometry affects the

13 lineshape of the $\bar{r}$=2.4 nm (20 mM) and the $\bar{r}$=3.0 nm (10 mM) samples, it proved difficult to

14 decisively determine estimates of the exact broadening parameter through comparison with

15 calculation. Spectra that demonstrate notable deviations from a typical derivative lineshape are

16 much easier to characterize. At lower concentrations the distinction between refractive

17 broadening and "true" linewidth broadening becomes subtle. Thus, we recognize that refractive

18 broadening is slightly broadening some spectra at $\bar{r}$=2.41 nm (20 mM) and $\bar{r}$=3.05 nm (10 mM),

19 where some variability of lineshapes is still observed, but make no attempt to quantify the correct

20 linewidth in these samples.

21 Nominally, we have only 2 variable parameters, the sample thickness (*d*) and the

22 resonance width (T_2). However, the measurement of the magnetic field is done through

23 calibration of the current in a superconducting sweep coil. Thus, the field calibration is not

24 precise enough to be used without modification, and so we must introduce a shifting parameter to

25 maximize overlap of the simulated to experimental spectrum. Finally, although the detection is

26 done in quadrature, the absolute phase is not precisely defined and depends on sample

27 temperature, room temperature and other parameters. Therefore, a 4th parameter is necessary to

28 match the phase shift of the collected data. In practice, the experimental spectra are first shifted

29 by hand in post-processing to roughly display a pure absorption and dispersion lineshape by

30 optimizing the symmetry of the spectra. Later, when calculated spectra are generated, their phase

31 and field offsets are varied to achieve maximum overlap with the experimental spectra (as

32 determined by the minimizing the difference between calculated and experimental spectra with

33 the Error discussed below).

34 As the phase and field shift are not meaningful parameters for this work, we seek only to

35 optimize them at each value of (T_2 , d), giving us a 2D parameter space to investigate. We adopt

36 the brute force method of generating a series of spectra spanning the reasonable values of these

37 two parameters and determining the error from the magnitude of the difference in real and

38 imaginary parts, i.e. Error $= \dfrac{\sum_n \sqrt{\left(X_{Exp}-X_{Calc}\right)^2+\left(Y_{Exp}-Y_{Calc}\right)^2}}{N_{Pts}}$

39

40 where X and Y represent the in phase and out of phase components, the subscripts Exp and Calc

41 referring to experimentally taken spectrum, and spectrum generated from the calculation outlined

1   above. The summation symbol indicates summation over all the points in the spectrum and N_{Pts}
2   is the number of data points. As the wings of the experimental lineshapes are not well described
3   by Lorentzians, the error was only calculated for the center of the spectra, defined by edges just
4   outside the extrema of the spectra. All the spectra (real and imaginary) are normalized by
5   intensity before they are compared.
6   We generated error landscapes for a range of parameters which reasonably covered the
7   experimentally possibly configurations. Specifically, sample thicknesses out to ~3 mm were
8   generally considered. However, no reasonable points were found beyond ~1.5 mm, which is
9   consistent with our expectations from sample volumes and holders. The sample thickness,
10   calculated based on the volumes assuming perfect, cylindrical packing were between 250 μm to
11   1.25 mm in the larger sample holder (~4 mm inner diameter) and was ~2.5 mm for the small
12   holder (~2 mm inner diameter). For the small sample holder (sample 4), the calculated sample
13   thickness was ~10x smaller than 2.5 mm, suggesting this estimation is inaccurate for this sample
14   setup. However, for the other samples (all measured in the larger sample holder), we find in
15   general that larger volumes lead to larger calculated thicknesses. However, the trend is neither
16   perfect, nor do the absolute thicknesses match, which can likely be explained by the fact that the
17   approximation of a flat sample is poorly realized given the high sample viscosity encountered
18   before freezing (resulting in a significant meniscus). While signal intensity does generally
19   increase with increasing volume, effects due to sample geometry and the short wavelength
20   compared to sample thickness (particularly for larger volumes) results in a nonlinear relationship
21   between signal strength and volume, and some variability is encountered based on the quality of
22   the loading.
23
24   As a general principle, we wished to investigate the local minima with values near to that
25   of the global minimum to determine if local minima provided better parameters estimates than
26   the global minimum, and to gauge the degree of confidence in our parameter estimates. We
27   restricted our investigation of minima to error values within 250% of the global minimum, to
28   screen only local minima which provide good agreement with the experimental lines. Thus,
29   much of the parameter space shown in forthcoming figures is "yellow" indicating a
30   comparatively high error value. In all cases, excepting one, the global minimum was retained
31   after reviewing the qualifying local minima. The evaluations of all five experiments are
32   presented below with a brief discussion in each case evaluating the reasonableness of the
33   parameters. In all cases, the parameters cited in the manuscript are those for the minima which
34   are boxed and have a blue arrow. These parameters are then used to determine the linewidth of
35   the susceptibility response, which is then the linewidth cited in the manuscript.
36

37   <u>Sample 1</u>
38   The first sample (shown in Fig. S2A) has a spectrum showing substantial deviation from
39   a single line, which generated an error landscape with a clear minimum value as shown in Fig.
40   S2B. Although another local minimum exists (located at d~1.3 mm, T_2~3.5 ns), the error value
41   was more than 50% higher than the chosen global minimum, and only the global minimum
42   reproduced the oscillations in the experimental lineshape well. Calculations with parameters near
43   this local minimum resulted in spectra with broader features, which smoothed out the oscillations
44   substantially. Thus, the robust global minimum located at d=928 μm and T_2=4.8 ns was used,
45   and the resulting calculated spectrum is shown in Fig. S2A.
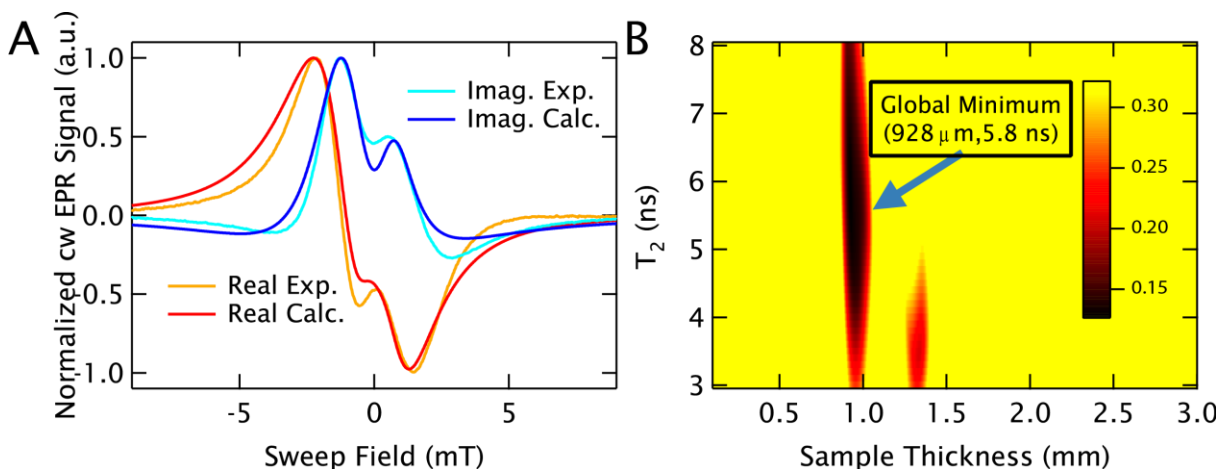46

Figure S2: Sample 1. A: The real and imaginary parts of the experimental spectrum (Real Exp. and Imag. Exp. respectively) are plotted for sample 1 ($\bar{r}$=1.8 nm (50 mM)) along with the spectrum calculated from the best fit parameters shown in **B** (Real Calc. and Imag. Calc. respectively). **B:** The error landscape for the experimental spectrum shown in **A** is plotted. The unusual lineshapes provide a simple landscape with one clear, robust global minimum, which described the spectral features better than the visible local minimum. The values of the minimum are shown in the boxed inset text with blue arrow, which provides the parameters for the calculated spectrum shown in **A**.

1   Sample 2
2   The experimental spectrum for sample 2 is shown in Fig. S3A and does not display
3   substantial deviations from a single line as was the case for sample 1, but rather is broadened by
4   the effects from refractive broadening. Fig. S3B shows an error landscape with both a global and
5   local minimum. Again, as expected from the error plots, we found that the local minimum
6   offered a less reliable fit, especially in the wings of the spectrum, where it was substantially
7   broader. Thus, the global minimum located at d=928 μm and T_2=4.8 ns was used, and the
8   resulting calculated spectrum is shown in Fig. S3A. However, the differences in lineshape
9   between the local and global minimum are not as drastic as in the previous case, where obvious
10   features were missing/obscured.
11
12   Sample 3
13   The spectrum of the third sample is presented in Fig. S4A and leads to a complicated
14   error landscape. Fig. S4B shows the error landscape with two different local minima in addition
15   to the global minimum. Although the local minimum at d=524 μm and T_2=3.9 ns produces a
16   lineshape with a higher error in the central part of the spectrum (compared to the global
17   minimum), it agrees slightly better in the wings. However, the two local minima and the global
18   minimum generate spectra which look largely similar; there are no distinguishing features (such
19   as oscillations) to help in discriminating between them. This helps demonstrate the subtlety of
20   the problem in the case of 'moderate' effects from refractive broadening, where the effect causes
21   some broadening of the line, but no dramatic change in the features. Essentially, the broadness of
22   the line can then result either from refractive broadening (which depend strongly on sample
23   thickness), or from dipolar broadening (which affects T_2). Given that our experimental lines are
24   already non-Lorentzian, we cannot distinguish well the best possible parameters easily.
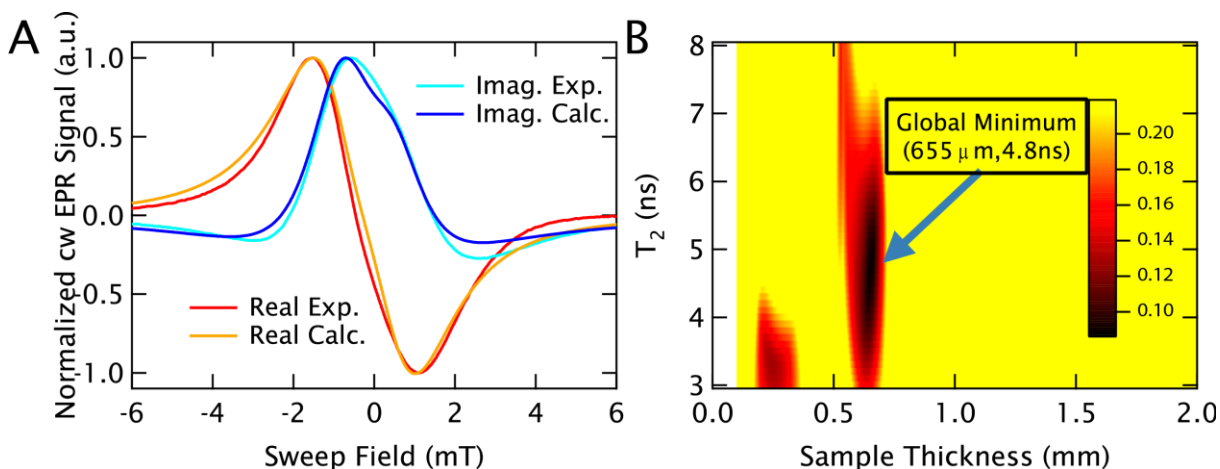25   However, we note that the volume for this sample was roughly ½ of that employed in sample 1

Figure S3: Sample 2. A: The real and imaginary parts of the experimental spectrum (Real Exp. and Imag. Exp. respectively) are plotted for sample 2 ($\bar{r}$=1.8 nm (50 mM)) along with the spectrum calculated from the best fit parameters shown in **B** (Real Calc. and Imag. Calc. respectively). **B:** The error landscape for the experimental spectrum shown in **A** is plotted. with a nearby local minimum with a value within 50% of the global minimum (in the lower left of the error landscape). However, as described further in the text, the global minimum better described the spectrum and so was used. The values of the minimum are shown in the boxed inset text with blue arrow, and provide the parameters for the calculated spectrum shown in A.

1   (Fig. S2), using the same sample holder, making d~500 μm a more reasonable physical estimate
2   of the thickness. Thus, facing the inability to clearly distinguish the quality of parameters purely
3   from the spectral comparison we reason that that the local minimum at d=524 μm and T_2=3.9 ns
4   gives a result which is consistent in terms of thickness and has comparable T_2 values with
5   previous results. Therefore is used as the most reasonable parameter values as shown Fig. S4A.
6
7
8   Sample 4
9   The spectrum of the 4th sample is shown in Fig. S5A. Although there are no dramatic
10   deviations from a single line, the error landscape in Fig. S5B offers a clear global minimum that
11   describes the lineshape well. The nearby local minima offer the correct qualitative lineshape, but
12   produce error values more than 50% great than the global minimum. In the absence of clear
13   distinguishing features of the experimental spectrum (such as oscillations), it is difficult to
14   determine the best spectrum by eye, and so we selected the global minimum at d=163 μm and
15   T_2=3.8 ns. Further, these local minima do not have substantially different T_2 values than the
16   global minimum, and so would not dramatically alter the estimated linewidth.
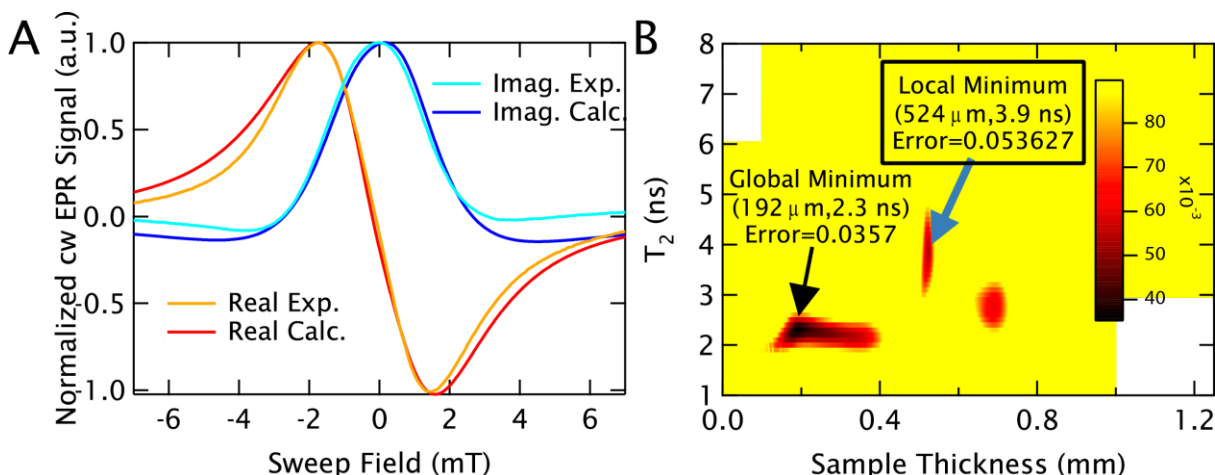17
18
19
20
21
22
23
24

Figure S4: Sample 3. A: The real and imaginary parts of the experimental spectrum (Real Exp. and Imag. Exp. respectively) are plotted for sample 3 ($\bar{r}$=1.8 nm (50 mM)) along with the spectrum calculated from the best fit parameters shown in **B** (Real Calc. and Imag. Calc. respectively). **B:** The error landscape for the experimental spectrum shown in **A** is plotted. The error landscape is more complicated than the previous two, with a two local minima which generate spectra similar to that of the global minimum. Although unequivocally justifying one set of parameters was not possible, the local minimum at d=524 μm and T_2=3.9 ns is reasoned in the text to be most consistent with previous results and so was chosen. The values of this minimum are shown in the boxed inset text with blue arrow, and provide the parameters for the calculated spectrum shown in A.

1
2   Sample 5
3   The 5th spectrum shows substantial deviations from a simple line as shown in Fig. S6A.
4   However, the error landscape, shown in Fig. S6B shows a deep global minimum, and two local
5   minima which also offer reasonable error values (at ~0.1 mm and 1.3 mm). However, local
6   minimum at d~0.1 mm does not produce any of the oscillations observed in the experimental
7   spectra. Alternately, the local minimum at d~1.3 mm does present some oscilations, but they do
8   not agree well with those observed in experiments. Thus, the global minimum at d=942 μm and
9   T_2=5.5 ns was used to determine the true linewidth in the presence of refractive broadening, as it
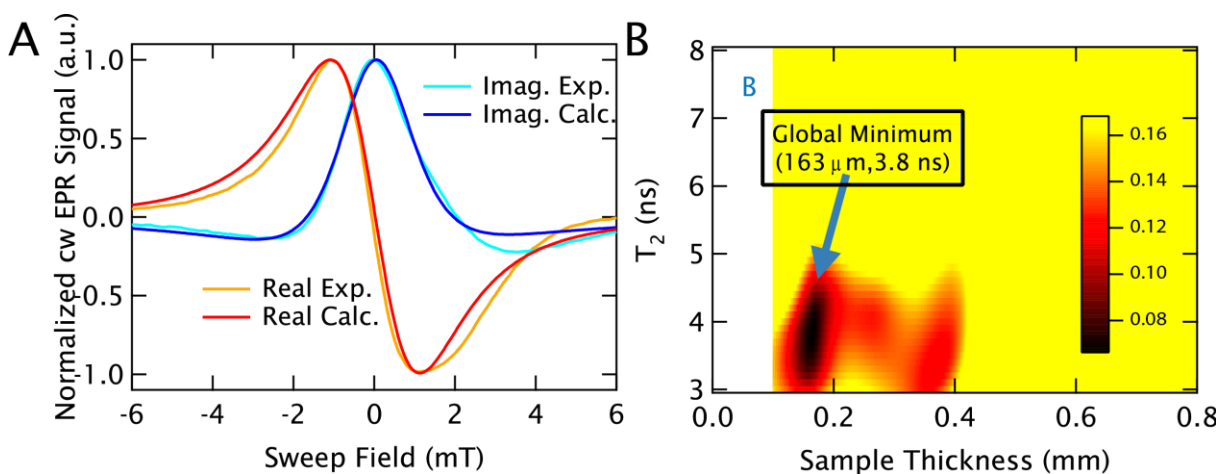10   describes the experimental spectrum well.
11

Figure S5: Sample 4. A: The real and imaginary parts of the experimental spectrum (Real Exp. and Imag. Exp. respectively) are plotted for sample 4 ($\bar{r}$=1.8 nm (50 mM)) along with the spectrum calculated from the best fit parameters shown in **B** (Real Calc. and Imag. Calc. respectively). **B:** The error landscape for the experimental spectrum shown in **A** is plotted. This error landscape offers a clear global minimum which describes the lineshape well, while the local minima present errors more than 50% above that of the global minimum. The values of the minimum are shown in the boxed inset text with blue arrow, and provide the parameters for the calculated spectrum shown in A.
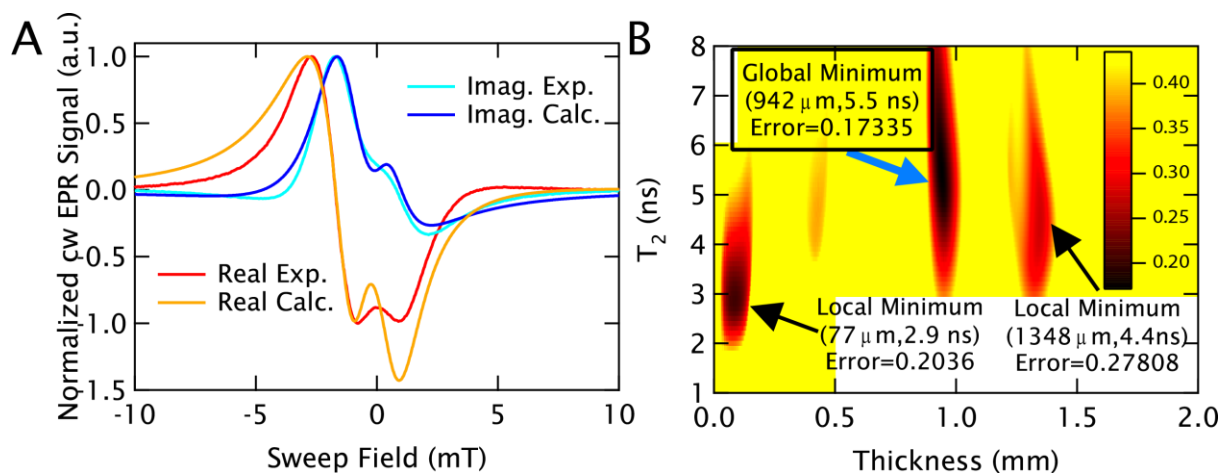
1
2

Figure S6: Sample 5. A: The real and imaginary parts of the experimental spectrum (Real Exp. and Imag. Exp. respectively) are plotted for sample 5 ($\bar{r}$=1.8 nm (50 mM)) along with the spectrum calculated from the best fit parameters shown in **B** (Real Calc. and Imag. Calc. respectively). **B:** The error landscape for the experimental spectrum shown in **A** is plotted. This error landscape offers a distinct global minimum and two local minima. Although the local minima both provide reasonable error values, neither describes the lineshape features properly, and so the global minimum is used. The values of the minimum are shown in the boxed inset text with blue arrow, and provide the parameters for the calculated spectrum shown in A.

3
4
5

1   Section 2: Temperature Dependent Pake Patterns

2   As discussed in the manuscript, the calculated broadening patterns are generated from
3   high-spin Pake patterns, which are then averaged over a distance distribution. The breadth of the
4   broadening is found to fall off with increasing temperature due to the changing of populations of
5   Zeeman states. This is shown in Fig. S7. The symmetric Pake pattern achieved at 260 K (where
6   the spin states are all similarly occupied) actually results in a narrower spectrum. This results
7   from the extremely high polarization of the |-5/2> and |-7/2> spin states at 10 K. These two states
8   have two of the broadest profiles, and so when polarized substantially, they produce very broad
9   effects. It is also interesting to note that at low temperatures the broadening is clearly shifted and
10   this should lead to a shift in the resonance going from 10 K to 260 K. This was not investigated
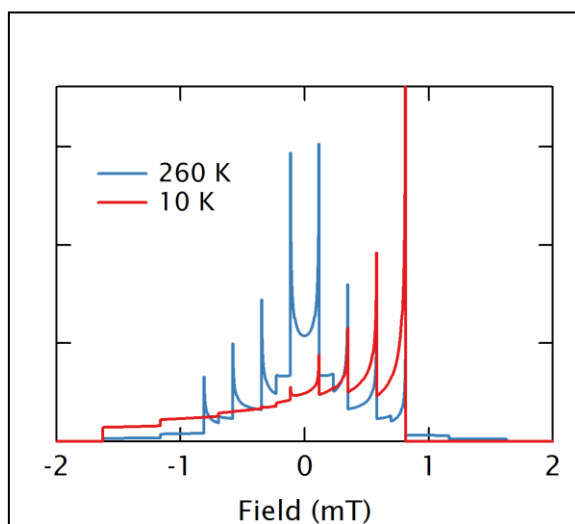11   in this study, as a field standard would be necessary.

Figure S7: Temperature Dependence of Pake Patterns. The Pake patterns describing the interaction of an S=7/2 ion interacting with an S=1/2 spin (as a model for observing only the central transition of the Gd^{3+} spectrum) at 10 K and 260 K. The far more symmetric pattern at 260 K actually leads to a narrower profile, which explains the reduction in broadening at 260 K.

Section 3: Estimation of Translational Correlation Time and Motional Averaging of the Dipolar Interaction

We can estimate the translational correlation times from literature where $\tau \approx a^2/D_f$ where a is the distance of closest approach for two Gadolinium and D_f is the diffusion constant of one complex relative to the other. Based on values in the literature[5], $\tau \sim 300 - 700$ ps at 298 K in water, which can be scaled by the approximate viscosity difference (140) to $\tau \sim 42 - 100$ ns. Previous work has shown that dipolar interactions in S=1/2 systems are sufficiently averaged when $\tau \geq$

$$\left(\frac{\frac{\mu_0}{4\pi(3\pi g^2 \mu_B{}^2)}}{r^3 h}\right)^{-1}$$, where μ_0 is the magnetic

constant, μ_B is the Bohr magneton, h is Planck's constant, and r is the interspin distance. This corresponds to when motion is slow enough that the strongest dipolar anisotropies are not averaged[6,7]. As in estimating the distance limits, we approximate the broadening of the S=7/2 to be ~3.5 times larger than for S=1/2, thus scaling the cutoff distance time by $(3.5)^{1/3}$, and suggesting that the dipolar interaction is static for distances shorter

34   than at least 4.1 nm (and up to 5.2 nm if the longer correlation time of ~100 ns is used).

35
36
37
38
39

1
2   **References**
3
4   1.   D. Friselli, C.-A. Massa, M. Martinelli, L. Pardi and I. Ricci, *Inorganica Chimica Acta*,
5   2008, **361**, 4164-4166.
6   2.   J. Jackson, *Classical Electrodynamics Third Edition*, Wiley1998.
7   3.   J. H. Jiang and D. L. Wu, *Atmospheric Science Letters*, 2004, **5**, 146-151.
8   4.   J. Solyom, *Fundamental of the Physics of Solids*2007.
9   5.   D. H. Powell, O. M. N. Dhubhghaill, D. Pubanz, L. Helm, Y. S. Lebedev, W. Schlaepfer
10   and A. E. Merbach, *Journal of the American Chemical Society*, 1996, **118**, 9333-9346.
11   6.   C. Altenbach, K.-J. Oh, R. J. Trabanino, K. Hideg and W. L. Hubbell, *Biochemistry*,
12   2001, **40**, 15471-15482.
13   7.   H. S. McHaourab, K. J. Oh, C. J. Fang and W. L. Hubbell, *Biochemistry*, 1997, **36**, 307-
14   316.
15